

# Porous, Superelastic NiTi Produced by Powder-Metallurgy

Scott M Oppenheimer<sup>1</sup>, John G. O'Dwyer<sup>2</sup>, David C. Dunand<sup>1</sup>

<sup>1</sup>Northwestern University; 2220 Campus Drive; Evanston, IL 60208; USA

<sup>2</sup> Waterford Institute of Technology; Cork Road, Waterford, Ireland

Subject Categories: Titanium, Shaping and Forming, Mechanical Properties, Powder Technology, Intermetallic

## Abstract

Near-stoichiometric NiTi was foamed in the solid state at elevated temperatures through creep expansion of high-pressure argon pores previously entrapped during powder consolidation. A sample with 17% porosity was found to be superelastic up to a compressive stress of 800 MPa.

## Introduction

Near-stoichiometric NiTi has been shown to be biocompatible [1], strong and yet elastically compliant [2]. After heat-treatment, slightly nickel-rich, NiTi exhibits superelasticity, a deformation mechanism relying on a reversible stress-induced transformation. Porous NiTi has good potential as a bone-replacement implant, since open porosity allows for bone ingrowth and also decreases the elastic modulus to values comparable to bone [3; 4]. Here, we demonstrate that the solid-state foaming process, used so far to produce Ti and Ti-6Al-4V with up to 50% porosity and tailorable ratios of open/closed porosity [5-7], can be employed to create porous NiTi.

## Experimental Procedures

Pre-alloyed equiatomic NiTi powder (particle size 44-177  $\mu\text{m}$ ) was roll-mixed with pure nickel powder to achieve an overall composition of Ni-49 at.%Ti, which is superelastic at room-temperature. These powders were then packed in a mild steel can (35 mm in diameter), which was backfilled with argon gas to a pressure of 2 or 4 atm and sealed by welding. The sealed cans were then hot isostatically pressed (HIPed) by UltraClad (MA), with the densified

billets being subsequently electro-discharge machined into small (~6mm) cubes for foaming.

As in the previous studies on Ti [5-7], the samples were heated to various elevated temperatures (between 1050 and 1200 °C) to allow for expansion of the high pressure argon pores by creep of the surrounding matrix, for times ranging from 8 to 36 hours. Some samples were foamed in a low-vacuum dilatometer which can produce a complete record of length vs. time. Residual gases however induced significant oxide formation on the surface, obscuring the expansion. To solve this problem, a high vacuum furnace was used with subsequent samples, which however did not allow for the record of a foaming curve. Melting was observed at the highest temperatures in both systems, at 1150 °C in low vacuum and 1200 °C in high vacuum.

Uniaxial compression testing was performed on a small foamed sample (3x3x6 mm) which had been solutionized in vacuum at 1000 °C for 4 h, quenched in chilled brine and aged in air at 400 °C for 4 h., prior to water quenching.

## Results and Discussion

The structure of the foamed samples was examined using standard metallographic analysis and synchrotron x-ray tomography. Both of these methods revealed initial stages of pore coalescence but the majority of the pores were isolated and generally equiaxed in shape. A comparison of the two methods can be seen in Figure 1. Whilst both images were taken from different regions of sample 1 (Table 1), they show generally the same structure, i.e. mostly equiaxed pores with little coalescence.

Table 1: Samples summary

Sample	Backfill Pressure (atm.)	Temperature (°C)	Vacuum (torr)	Time at Temperature (h)	Final Porosity (%)
1	2	1105	$10^{-3}$	8	17
2	2	1050	$10^{-3}$	16	17
3	2	1100	$10^{-6}$	36	14.5
4	2	1150	$10^{-6}$	16	13.5
5	4	1150	$10^{-6}$	16	13

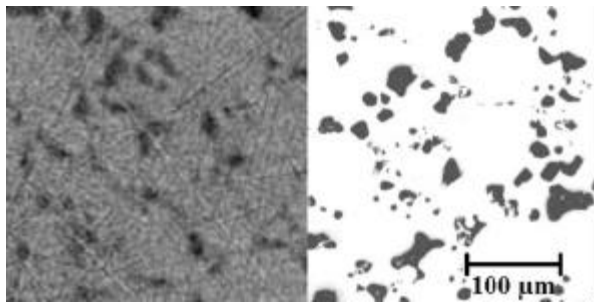


**Figure 1 - X-Ray micro-tomography (left) and optical microscopy (right) cross-section of sample 1, with 17% porosity (same magnification).**

A three-dimensional reconstruction of the tomography data is shown in Figure 2. The lack of large-scale pore coalescence implies that Ar is still present within the pores and has not escaped to the surface. This indicates that additional foaming and enhanced porosity could be achieved by further exposure to similar or higher temperatures.

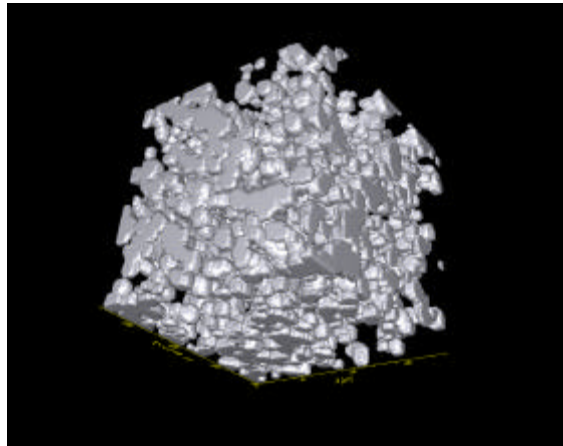


**Figure 2 - Three-dimensional re-construction of sample 1 with 17% porosity from x-ray tomography; the cubic volume shown is 360μm on each side.**

The compressive stress-strain behavior of a specimen taken from sample 1 is shown in Figure 3, which incorporates three load-unload loops. Superelastic recovery is apparent for all three unload branches, and reaches a value of ca. 7% for the third loop. Also noteworthy is the low value of the apparent modulus of elasticity on loading (outside the loops) of 9 GPa, which is within the range found for bone (5-20 GPa). This low value cannot be fully explained by porosity, and is indicative of linear superelasticity. Direct proof of superelastic behavior on loading and unloading will be provided by *in-situ* synchrotron experiments, as previously undertaken on bulk NiTi samples [8]. The present foams, with rounded pores and mostly closed porosity, show very high strengths (>800 MPa, Fig. 3), which are unlikely to be achieved in sintered NiTi foams because of their open porosity and weak sintering necks.

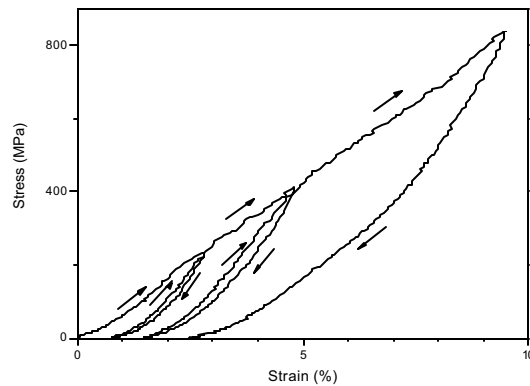


**Figure 3 - Compressive stress-strain curve for sample 1 with 17% porosity, showing three load-unload loops and superelastic behavior.**

### Conclusions

Powder metallurgy was used to create a NiTi billet with pressurized Ar pores, which were subsequently expanded at elevated temperature to a volume fraction of 17%. The NiTi foam exhibited linear superelasticity with a low apparent elastic modulus (9 GPa) and a high strength (>800 MPa). Higher levels of open porosity should be attainable through the judicious selection of compaction and foaming parameters, thus enabling novel superelastic bone implants with low stiffness, high strength, excellent biocompatibility and good bone-anchoring capability.

**Acknowledgments** – We acknowledge support from NSF (through grant DMR-0108342/001) and from Enterprise Ireland (for JOD) through its International Collaboration Programme. We also thank Prof. P. W. Voorhees for use of visualization software. Use of the Advanced Photon Source was supported by the U. S. Department of Energy, Office of Science, Office of Basic Energy Sciences, under Contract No. W-31-109-Eng-38.

### References

- [1] M. Sigler, S. Handt, M.C. Seghaye, G. von Bernuth, R.G. Grabitz, Heart 83 (2000) 570-573.
- [2] B.Y. Li, L.J. Rong, Y.Y. Li, Intermetallics 8 (2000) 643-646.
- [3] D.C. Lagoudas, E.L. Vandygriff, Journal of Intelligent Material Systems and Structures 13 (2002) 837-850.
- [4] D.S. Grummon, J.A. Shaw, A. Gremillet, Applied Physics Letters 82 (2003) 2727-2729.
- [5] M.W. Kearns, P.A. Blenkinsop, A.C. Barber, T.W. Farthing, International Journal of Powder Metallurgy 24 (1988) 59-64.
- [6] N.G.D. Murray, D.C. Dunand, Composites Science and Technology 63 (2003) 2311-2316.
- [7] N.G. Davis, J. Teisen, C. Schuh, D.C. Dunand, Journal of Materials Research 16 (2001) 1508-1519.
- [8] A. Schuster, H.F. Voggenreiter, D.C. Dunand, G. Eggeler, Journal De Physique IV 112 (2003) 1177-1180.